12

Technological Aspects of Scalable Processes for the Production of Functional Liposomes for Gene Therapy

Julia E. Trevisan[1], Leide P. Cavalcanti[2], Cristiano L. P. Oliveira[3], Lucimara G. de La Torre[1] and Maria Helena A. Santana[1]
[1]*University of Campinas*
[2]*Brazilian Synchrotron Light National Lab*
[3]*University of São Paulo*
Brazil

1. Introduction

The success of gene delivery systems in *in vivo* or *in vitro* applications depends on efficient transfection. Cationic liposomes remain a promising alternative for nonviral DNA carriers, mainly because they protect DNA from interstitial fluids and easily interact with cells (Gregoriadis, 1993; Lasic, 1997). However, in order to be effective in the immunological response, cationic liposomes must be functional and reach their specific target. Stability, reduced toxicity, efficiency in delivering genes to cells, and specific targeting to the nucleus are essential requirements for prophylactic and/or therapeutic performance. In order to achieve these standards, important physico-chemical parameters in liposomes must be controlled, such as the functionality of the lipids, the concentration of the cationic lipid, DNA loading (reflected by the $R_{+/-}$ molar charge ratio), the zeta potential, size, and polydispersity.

Several laboratory experiments have already explored DNA vaccines using cationic lipids. A classical investigation of lipid functionality and composition, as well as the efficiency of cationic liposomes as DNA carriers, was performed by Perrie and colleagues (Perrie & Gregoriadis, 2000; Perrie et al., 2001). The plasmid pRc/CMV HBS encoding the S (small) region of hepatitis B surface antigen was encapsulated in dehydrated-hydrated liposomes composed of egg phosphatidylcholine (EPC, bilayer-forming lipid), 1,2-dioleoyl-3-trimethylammonium-propane (DOTAP, cationic lipid), 1,2-dioleoyl-*sn*-glycero-3-phosphoethanolamine (DOPE, helper lipid) in a 50:25:25 percent molar ratio. The authors demonstrated that the encapsulation process protects the DNA vaccine against incubation with sodium dodecyl sulfate (SDS) due to DNA incorporation inside the liposome lamella (Perrie & Gregoriadis, 2000), and a better immunological response was obtained with cationic liposomes compared to naked DNA.

Concerning size and polydispersity, different authors have reported that nanoparticle size is an important parameter for transfection success (Ma et al., 2007; Ogris et al., 1998; Rejman et al., 2004; Ross & Hui, 1999; Wiewrodt et al., 2002). Indeed, most of the variability in transfection procedures is a consequence of non-viral gene delivery systems with high polydispersity index values. The polydispersity index is related to the width of the particle

size distribution. High polydispersity indicates that greater population fractions are out of the optimum size range for cell transfection (Hsieh et al., 2009).

In this sense, a rational design associated with a technological process able to construct functional liposomes efficiently is needed. Otherwise, the technological processes must be scalable in order to guarantee the reproducibility of the formulation when more liposomes have to be produced for pre-clinical and clinical assays before industrial production. In addition, deep understanding of the phenomena involved, as well as the correlation among operational variables and the physico-chemical parameters, allows more precise control of the quality of the final product and a rational optimization of the process. Therefore, process and product must be strongly linked to assure the desired biological performance.

The literature reports valuable results regarding the biological performance of cationic liposomes in vaccination and gene therapy. However, to the best of our knowledge, no study has yet focused on the approach connecting design, product, and production process. We obtained promising immunological responses and a prophylactic effect against tuberculosis (TB) using cationic dehydrated-hydrated liposomes (DRV) complexed to DNA containing the hsp65 gene on the external surface (Rosada et al., 2008). Hsp65 is a heat shock protein from *M. leprae*. The hsp65 gene has been extensively studied and its biological effects evaluated for protection against and the treatment of tuberculosis (de Paula et al., 2007; Silva et al., 2005). Formulations based on the hsp65 gene have been used in different immunization strategies and the evaluation of protection against *M. tuberculosis* challenge (Souza et al., 2008).

We developed a novel and non-toxic formulation of cationic liposomes in which the hsp65 DNA vaccine was entrapped or complexed on the external surface of the cationic DRV. The formulation was used to immunize mice by intramuscular or intranasal routes. A single intranasal dose of the formulation elicited humoral and cellular immune responses that were as strong as those induced by four intramuscular doses of naked DNA in the mouse model of TB. The formulation also allowed a 16-fold reduction in the amount of DNA administered. Moreover, this formulation was demonstrated to be safe, biocompatible, stable, and easy to manufacture at low cost. We think that this strategy can be applied to human vaccination against TB in a single dose or in prime-boost protocols with a tremendous impact on controlling this neglected disease (Rosada et al., 2008).

The net positive surface charge imparted by DOTAP drives electrostatic binding to the cell membrane. The fusogenic properties of phosphatidylethanolamine promote the exchange of lipids with the endosomal membrane and delivery of DNA into the cytoplasm (Xu and Szoka, 1996). Finally, the presence of EPC provides stability to the liposomes, reduces the cytotoxicity of the cationic lipids, and delimits the diameter of liposome construction, which influences macrophage phagocytosis. For the same lipid composition, the complexation of DNA on the surface of liposomes generated more cell accessibility (non-electrostatically bound DNA) to DNA in relation to encapsulated DNA, and controlled antibody production related to DOTAP/DOPE lipoplexes (de la Torre et al., 2009). The liposomes were prepared using Bangham's method (Bangham et al., 1965) and characterized according to size, polydispersity, and zeta potential. DNA loading and availability on the external surface of liposomes were also determined (Rosada et al., 2008).

For the next pre-clinical and clinical assays, a scalable process had to be established in order to evaluate the capability of the system in scale transposition, reproducing the physico-chemical and biological properties of the previously prepared liposomes on a laboratory scale.

In this chapter, we review the top-down and bottom-up approaches for liposome production and DNA complexation aiming at gene vaccines. The technological processes are classified into strategies and the feasibility to scale transposition envisaged. The physico-chemical aspects of the processes and properties of the produced liposomes are correlated, connecting product and process. In addition, we report our experience with a scalable production of previously designed cationic DNA-EPC/DOPE/DOTAP liposomes in a top-down process involving ultra-turrax and microchannel microfluidizer devices for the homogenation and reduction of liposome size.

2. Liposomes: Structure, formation, and characterization

In general, amphiphile molecules, when dispersed in a liquid medium, undergo internal self-organization, generating colloidal aggregates. Liposomes are formed through the aggregation of phospholipid molecules in an aqueous medium. Initially, a plain bilayer structure is formed when the relative volumes between the non-polar and polar parts of the phospholipid molecules are favorable (packing factor is close to 1) for vesiculation in closed structures. The timing of spontaneous self-aggregation is long, and in technological processes this time is reduced by promoting vesiculation via the addition of energy to the system and remotion of the organic solvent or detergent in which the lipids were initially dispersed (Gregoriadis, 1990; Lasic, 1993). Primary aggregation generates unilamellar liposomes, which undergo secondary aggregation, forming multilamellar liposomes (Figure 1).

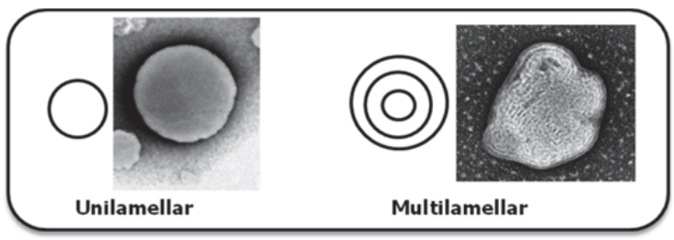

Fig. 1. Unilamellar and multilamellar liposomes.

The main physico-chemical characterization of cationic liposomes for gene vaccines includes average hydrodynamic diameter and size distribution, zeta potential, and morphology. These characterizations have been well described in the modern literature, including techniques, equipment, and the software used for analyzing data.
Regarding the average hydrodynamic diameter and size distribution, photon correlation spectroscopy (PCS) and dynamic laser light scattering using a Ne-He laser are generally used for measurements at various incidence angles. Particle diameter is calculated from the translational diffusion coefficient using the Stokes-Einstein equation:

$$d(H) = (kT)/(3\pi\eta D) \quad (1)$$

Where d(H) is the hydrodynamic diameter, D is the translational diffusion coefficient, k is Boltzmann's constant, T is the absolute temperature, and η is the viscosity. The mean diameter and size distribution are estimated by an adequate algorithm analysis. The results of the population distributions are expressed as the intensity of scattered light and automatically converted to number-weighted mean diameter and size distribution by adequate software. For more accurate size characterization, intensity and number-weighted

mean diameters are considered. Although the whole range of diameters is shown in the intensity-weighted distribution, the proportionality to the sixth power of particle diameter underestimates small particles, which are only very weakly weighted (Egelhaaf et al., 1996). The corresponding number-weighted distribution converted using the Mie theory is in equivalent proportion to the first power of the diameter and determines the actual number of particles yielding the observed intensity in each size class (Hulst, 1969).

Several structural parameters involved in the process of liposome preparation can be studied and controlled using X-ray techniques. The simple piling of several polar lipid bilayers produces an X-ray diffraction pattern from which one can determine the periodicity, the type of lattice, and an estimate of water molecules in the interface. The colloidal size of self aggregates, such as the dispersion of liposomes, can be characterized by small angle X-ray scattering techniques directly in the liquid buffer media, complementing some indirect microscopy methods (Kratky 1988). Structural phase transition, swelling, crystallization, permeation, nucleation, and other properties will be reflected in a change in the scattering pattern. More than a few dimensions in polar lipid/water systems, such as, lattice periodicity and arrangement, aggregate size, and defects, are on the order of magnitude of the X-ray wavelength, a few Angstroms. The bigger the particle (up to a few hundred Angstroms), the smaller the scattering angle. The terms small angle X-ray scattering (SAXS) and wide angle X-ray scattering (WAXS) are applied. X-ray diffraction is a particular case of scattering for ordered systems.

2.1 Small angle X-ray scattering (SAXS)

Here, we present an outline of the main features of the general X-ray techniques applied specifically to the case of liposome characterization. For better comprehension of the theory of X-ray scattering, the reader may like to consult the works of Glatter (Glatter & Kratky 1982, Glatter 1991) and Kratky (Kratky & Laggner 2001). For the notation, as a convention in the literature, and in order to avoid dependence on wavelength values, the scattering angle is normalized using the following equation:

$$q = |\mathbf{q}| = \frac{4\pi}{\lambda} \sin\theta \tag{2}$$

Where q is the wave vector, 2θ the scattering angle, and λ the incident wavelength. By using the wave vector instead of angles, one can directly compare experiments performed with different X-ray wavelengths. SAXS is the elastic scattering that occurs when X-rays strike a sample of given material. The electrons of each atom in the sample will re-emit the same energy isotropically. The total scattering amplitude, or amplitude "form factor" F(q), is a sum of all scattered waves in all directions as defined in Equation 3,

$$F(\vec{q}) = \int \rho(\vec{r}) e^{-i\vec{q}\cdot\vec{r}} d\vec{r} \tag{3}$$

Where $\rho(\vec{r})e^{-i\vec{q}\cdot\vec{r}}$ is the amplitude of the wave scattered by an atom located at position r. The result is a maximum intensity in the direction of the incident beam decreasing smoothly as a function of the scattering angle. The intensity of the scattering will depend directly on the electronic density $\rho(\vec{r})$ of the sample, i.e., the number of electrons per unit of volume. More specifically, for our case, the higher the difference between the electronic densities of the scattering centers of the sample (e.g., liposomes) and the media (e.g., buffer solution), the

higher the total scattering intensity. Lipid/water systems generally contain light atoms (low atomic number) and, consequently, very low electronic density contrast. A way to increase the scattering intensity is to use high flux X-ray sources, such as synchrotrons. The SAXS experiment will give information on the particle/system structure. Usually, the main goal of the SAXS analysis is the determination of the electron density $\rho(\vec{r})$. This is the so called inverse scattering problem since the information is given in reciprocal space. There are several procedures that can be applied to determine $\rho(\vec{r})$. One possible approach is the calculation of a theoretical intensity obtained for an assumed model object and the comparison to the experimental data. The more information one has about the sample, the more consistent the model will be and, consequently, the simpler the SAXS analysis. Nevertheless, some parameters can be determined directly from the scattering curve, for instance, the radius of gyration of a particle, Rg, which is the root mean square of the distances of all electrons from the center of gravity of the particle. The Rg is determined using the Guinier method, which approximates the scattering function to a simple distribution in the limit of very small angles (q~0.01Å^{-1}). A graph plotting ln I(q) versus q^2 in the limit for very low angles might be characterized by a straight line with an angular coefficient proportional to Rg^2.
Considering that the particles are spheres with radius r, it yields:

$$R_g{}^2 = \frac{3}{5} r^2 \tag{4}$$

The two requirements for using Guinier approximation are: the sample should be a monodisperse colloidal system, which implies no interaction between the scattering centers, and the experimental data must have a minimum q such that $d<\pi/q$, where d is the maximum particle dimension that can be studied (Glatter 1982). For systems of large unilamellar vesicles in which the dimensions of the particles are not inside the limit of SAXS experiments, other methods, such as visible light scattering, can be used (Glatter 2002). In some cases, determining the cross section distance would be interesting, such as in large unilamellar vesicle systems, where the thickness of the lamellae is inside the limits of the Guinier approximation. In this case, the graph of $I(q)q^2$ versus q, called the "thickness Guinier plot", is used to determine the radius of gyration of the thickness RT com $RT = T/\sqrt{12}$, were T is the bilayer thickness). Another approach is to obtain the electron density across the thickness of the vesicle, $\rho_t(x)$. The latter approach can be applied both for unilamellar of multilamellar vesicles as will be discussed next.

2.2 X ray diffraction (XRD)

Diffraction can be viewed as a particular case of scattering: Due to the periodicity, d, of the system, the sum or integration of all scattered intensities turns into an interference pattern. In analogy, the function S(q) which is the result of the integration, is called the "structure factor". The scattering curve, or diffraction pattern, presents peaks for certain scattering angles, θ, which can satisfy Bragg's condition (Azaroff 1968):

$$n\lambda = 2d\sin\theta \tag{5}$$

Where λ is the wavelength of the incident X-ray beam and n is the order of diffraction. We can observe a diffraction pattern, for example, in multilamellar lipid vesicles, which have a

lipid bilayer periodicity on the order of 50 Å. The determination of the period of the bilayer is useful for characterizing the structural phase of the system and its transitions. If several orders of diffraction are observed, the structure factor function can be reconstructed and the electronic density profile of the lipid bilayer determined (Pachence & Blasie 1991). The incorporation of compounds inside the lipid bilayer can alter the density profile and be controlled (Sato et al. 2009). Also the matrix of acyl chains is a periodic arrangement with distances between chains on the order of 5 Å. The determination of this parameter is helpful for controlling the stability of the liposome. Any change in these distances will be followed by a dislocation of the diffraction peak.

2.3 Simultaneous determination of form factor and structure factor

Some systems present both form factor and structure factor. The scattering intensity from such a system can be written by the following expression:

$$I(q) = c\left\langle P(q)S(q)\right\rangle \tag{6}$$

Where c is related to the concentration of particles in the system, $P(q)=|F(q)|^2$ is the intensity form factor of the particles and carries information about particle shape and contrast and S(q) is the system structure factor, which carries information about possible interparticle interactions or arrangements. The brackets "$\langle\ \rangle$" indicate that in the general case these two contributions have to be averaged together in the calculation. For highly anisotropic systems, like vesicles for example, where the transversal dimensions are much larger than the perpendicular dimension, the form factor can be considered as only corresponding to the perpendicular direction (1D function) and equation 6 can be rewritten as,

$$I(q) = \frac{c}{q^2}\left\langle P(q)S(q)\right\rangle \tag{7}$$

One usual approach is to use the decoupling approximation and treat the form factor and structure factor separately. For a lamellar system, the structure factor is well described by the MCT theory (Zhang et al. 1994)

$$S(q) = 1 + 2\sum_{n=1}^{N-1}\left(1-\frac{n}{N}\right)\cos(nqd)\ e^{-(d/2\pi)^2 q^2\eta\gamma}(\pi q)^{-(d/2\pi)^2 q^2\eta} \tag{8}$$

The average number of coherent scattering bilayers in the stack is denoted as N, γ is Eulers' constant and d the separation between layers. The Caillé parameter η involves both the bending modulus K of lipid bilayers and the bulk modulus B for compression (Caille 1972, Zhang et al. 1994).

$$\eta = \frac{\pi\ k\ T}{2d^2\sqrt{BK}} \tag{9}$$

The description of the form factor can be done in several levels of detail. One of the simplest approximations is to consider a two step model given by (Nallet et al. 1993),

$$P(q) = \frac{4}{q^2}\left\{\Delta\rho_H \sin\left[q\left(\delta_H+\delta_T\right)\right] - \Delta\rho_H \sin\left(q\delta_T\right) + \Delta\rho_T \sin\left(q\delta_T\right)\right\}^2 \tag{10}$$

Where $\Delta\rho_H$ and $\Delta\rho_T$ are respectively the head group and tail group electron density contrasts and δ_H and δ_T are the sizes of the head group and tail group. Following the step model strategy, Glatter and co-workers developed the deconvolution square root method (Glatter & Kratky 1982, Fritz & Glatter 2006) where the electron density is described by several step functions and it is applied a constrained least squares fitting routine to obtain the step heights.
Another strategy was proposed by Pabst et.al (Pabst et al. 2000), which models the bilayer using a two Gaussian system: a central Gaussian placed at the origin, which can model the central part of the tail groups, and is known to have negative contrast with respect to a water buffer (when using X-Rays), and a second Gaussian placed at a certain distance Z in such a way that it can model the position of the head group region. This approach and the two step model cannot describe high quality data, principally for high q values (Oliveira et al. Unpublished work). In a recent development, Oliveira and co-workers combined the advantages of the Gaussian description with the stability introduced by the Glatter method, enabling a more flexible and stable model procedure.
In this approach the profile is described by a symmetric sum of several equally spaced Gaussian functions. The amplitude of each Gaussian is smoothened by extra constraints. The constraints are used to ensure the numerical stability of the nonlinear least-square fit. By proper choice of the amplitude of each Gaussian it is possible to build a smooth profile that can describe more accurately the electron density of the bilayer. Usually, 4 Gaussians function are sufficient to describe a bilayer profile satisfactorily. The electron density is defined as

$$\rho(z)=\sum_{n=1}^{4} a_n\left[G_s(z,z_n,\sigma_n)+G_s(z,-z_n,\sigma_n)\right]/\left(1+\delta_{i1}\right) \qquad \begin{matrix}\delta_{i1}=1, i=1\\ \delta_{i1}=0, i=2,3,4\end{matrix} \tag{11}$$

$$G_s(z,z_n,\sigma)=\frac{1}{\sigma\sqrt{2\pi}}\exp\left[-(z-z_n)^2/2\sigma^2\right] \tag{12}$$

and the Kroninger delta function δ_{i1} is used to avoid double counting for the central Gaussian. n is the order of Gaussian used. The profile is defined by the values of the amplitude factors a_n. Given a half bilayer thickness Z the centers of the Gaussians and the standard deviations (σ values) are defined as follows:

$$z_n=(n-1)2\sigma, \qquad \sigma=\frac{Z}{2n_{\max}\sqrt{2\ln 2}} \tag{13}$$

This choice of the centers and standard deviations gives a reasonable overlap between the Gaussian functions enabling the construction of smooth profiles. A typical profile built using equation 11 is shown in the figure 2 (left). One of the advantages of using a Gaussian set of functions for the representation of the profile is that, for the one-dimensional case of centro-symmetric bilayers, the integral in equation 3 has one analytical solution, given by:

$$F(q,n)=\sqrt{2\pi}\sigma\exp\left(-\frac{\sigma^2q^2}{2}\right)\cos(q\,z_n) \tag{14}$$

The final scattering amplitude is just the addition of all the F(q,n) terms:

$$F(q)=\sum_{n=1}^{4} a_nF(q,n) \tag{15}$$

Regardless the methodology to calculate the form factor, this procedure gives the scattering contribution from the built shape of the electron density profile. For the multilamelar vesicles this profile will be a repeating unit for each vesicle layer. By using the structure factor given from the modified Caillé theory (equation 8), the final scattering intensity is then given by:

$$I_{MLV}(q) = \left(\left| F(q) \right|^2 S_{MCT}(q) + N_{diff} \left| F(q) \right|^2 \right) \tag{16}$$

Where the second term gives rise to a diffusive scattering which might appear from the presence of single bilayers in the sample. Smearing effects, which are a consequence of the collimation of the camera pinholes, wavelength bandwidth, detector resolution, etc, can be taken into account by the use of the resolution function R(⟨q⟩,q), as described in the work of Pedersen (Pedersen et al. 1990). The final expression used to describe the data from multilamellar vesicles is given by:

$$I(q)_{FIT} = Sc_1 \frac{I_{MLV}(\langle q \rangle)}{q^2} + BG \tag{17}$$

Sc_1 is an overall scale factor and BG is a constant background. Both are optimized during data fitting. Using the above mentioned procedure it is possible to perform a full curve fitting, retrieving simultaneously information about the form factor and structure factor. A simulated example and an application to real experimental data are shown in Figure 2(right).

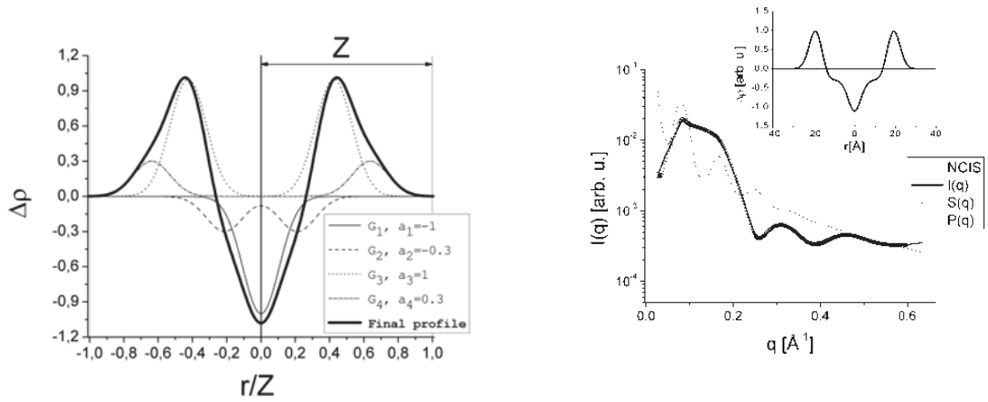

Fig. 2. Left: Construction of the electron density profile using four Gaussians (G1, G2, G3 and G4) with four different amplitudes (-1, -0.3, 1, 0.3). They are shown in four different lines. The final resultant electron density profile from the Gaussian model is shown in solid thick line. Right: Fitting of experimental data using the 4-Gaussians approach. Open circles: experimental data for Egg phosphatidylcholine (EPC) liposome system. Solid curve: Theoretical intensity I(q). Dotted line: structure factors S(q). Dashed line: intensity form factor P(q). The obtained number of layers was N=50, Interplanar distance d=73.5±0.2Å, Caillé parameter of η=0.13±0.01 and bilayer half size of Z=30.00±0.06Å. The obtained electron density profile is shown in the inset.

3. Top-down and bottom-up approaches in processes

In general, the processes for producing nanomaterials can be characterized as two main approaches, top-down or bottom-up. The top-down approach starts with large particles that are comminuted to a nanometric size through the application of high-energy forces. This is the classical approach for the majority of nanoparticle production processes. Top-down approaches require highly precise control of the variables of the process in order to obtain the narrow particle size (Mijatovic et al., 2005). Lithography is the classical example. Other high-energy processes include grinding, high impact homogenization, ultrasound waves, and extrusion through nanoporous membranes (Sanguansri & Augustin, 2006).
Bottom-up approaches are based on the self-organization of molecules under thermodynamic control, generating nanostructures from atoms and molecules as a result of the effects of the chemical, physical, and process interventions on the balance of the intermolecular and intramolecular forces of the system components (Sanguansri & Augustin, 2006). Bottom-up approaches focus on the construction of functional materials, mimetizing the hierarchic organization of the molecules in live organisms, though the science still does not dominate the complex auto-aggregate structures in nature.
Regarding liposome production, top-down approaches comprise the high-energy comminution of a polydispersed population of multilamellar liposomes formed under non-controlled aggregation. The bottom-up approach manipulates the phospholipid molecules in controlled local aggregation in space and time, generating a monodispersed population of nano-sized unilamellar liposomes. Figure 3 illustrates top-down and bottom-up approaches for liposome production.

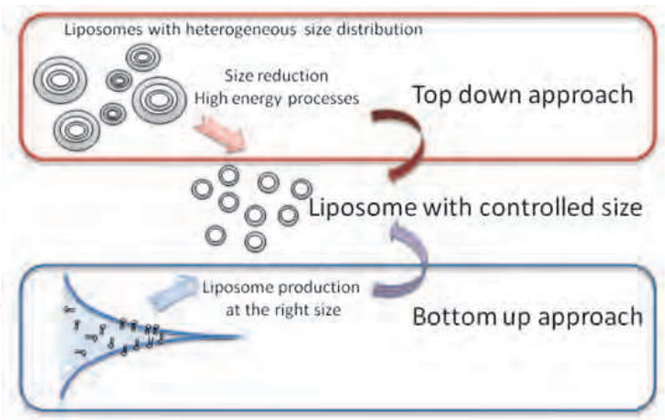

Fig. 3. Scheme of top-down and bottom-up approaches for liposome production.

4. Technological processes

Most of the conventional methods for liposome production require an additional unit operation for size reduction and polydispersity, as they are top-down approaches. In this approach, liposomes are produced from the hydration of a thin film of lipids using Bangham's method (Bangham et al., 1965), multitubular system (Torre et al., 2007; Tournier et al., 1999), detergent depletion or emulsion methods, ether/ethanol injection, and reverse phase evaporation (Lasic, 1993; New, 1990). All of these processes are discontinuous and only the ether/ethanol injection and multitubular system are scalable. Shearing or impact strategies are

the general key for homogenation and reducing liposome size. Mechanical stirring, extrusion through orifices (French press), extrusion through membranes, high-pressure impactor, and microchannel microfluidizer are equipment used in high-energy processes.
Bottom-up processes are low energy processes inspired by biological systems and used for the development of functional nanomaterials, such as supramolecular structures, self-aggregated monolayers, Langmuir-Blodgett films, aggregated peptide nanotubes, and deposited polyelectrolites or proteins in multilayers (Mijatovic et al., 2005; Shimomura & Sawadaishi, 2001).
Microfluidic systems have been the main representatives of bottom-up processing for liposome production in continuous and scaled up processes. Different microfluidic systems can be applied to the production of liposomes and giant liposomes (Ota et al., 2009; Shum et al., 2008; Wagner et al., 2002). DNA complexation on the external surface of liposomes also constitute a promising technology for the production of gene vaccines.

4.1 Microfluidic systems for the production of cationic liposomes

Among different microfluidic geometries, hydrodynamic focusing (HF) is a promising technology and liposomes can be produced in sizes ranging from 50 to 500 nm (Jahn et al., 2004, 2007; Wagner et al., 2002). The HF consists of a device with four-microchannel intersection geometry (Figure 4A). The organic solvent, miscible in water (isopropanol, ethanol), containing dispersed lipids are injected in the middle stream and hydrodynamically compressed by two aqueous (or buffered) streams. The precise upstream flow rates are achieved using syringe pumps that control the position of the focused stream in the downstream channel and, consequently, the process quality parameters (Baldas & Caen, 2010). The use of stereo microscopy is recommended to monitor the process as presented in the schematic representation of the experimental apparatus in Figure 4B. The laminar flow rate allows the formation of a well defined region between the two miscible fluids. The interfacial forces between two miscible solvents (for example, water and isopropanol or water and ethanol) control the convective-diffusive process and liposome self-assembly (Jahn et al., 2010). From the phenomenological point of view, the continuous flow mode allows the continuous diffusion of water and alcohol, reducing lipid solubility, which causes thermodynamic instability and generates liposomes (Jahn et al., 2008). The continuous flow mode also increases productivity.
The HF geometry for liposome production is based on the conventional method of ethanol injection (bulk) adapted for microfluidic systems. Conventional ethanol injection consists of the controlled addition of an ethanol/lipid stream in a tank reactor containing buffered water under controlled agitation. The advantage is the use of ethanol; compared to other organic solvents (e.g., chloroform and methanol), it is less harmful and, depending on the lipid concentration, there may be no need for post-treatment size reduction (Kremer & Esker, 1977). Some of the disadvantages are low lipid concentration in ethanol (higher concentrations require post-treatment for size reduction) and a difficulty achieving reproducibility (Wagner et al., 2002).
The representative parameters for liposome size and polydispersity control in HF are channel geometry (deep and width), volumetric flow buffer/alcohol rate-ratio (FRR), and total volumetric flow rate (buffer+alcohol flow rates). Solvent diffusivity in water is another important parameter (Jahn et al., 2004, 2007, 2010). Basically, the narrower the microchannel width, the smaller the liposome size. For total volumetric flow rate, which promotes flow velocity at the channel, higher FRRs (which corresponds to an increased proportion of buffer

to lipid/solvent flow) correspond to smaller liposome diameter (Janh et al., 2010). However, caution is required in this flow rate analysis as the final alcohol content in the liposome colloidal dispersion can change with FRR and as a consequence of particle size. Alcohol can be used to disrupt liposomes and, at low concentrations, liposome size can be increased due to alcohol incorporation into the bilayer. Precise analysis can be performed if the alcohol is removed after liposome processing. By decreasing the total volumetric flow rate, the residence time can be increased and a lower average vesicle diameter and narrower size distribution obtained. This behavior indicates that if increasing the total volumetric flow rate, the microchannel length must be longer to complete the alcohol diffusion, otherwise large particles will be obtained due to bulk mixing downstream of the channel (Janh et al., 2010).

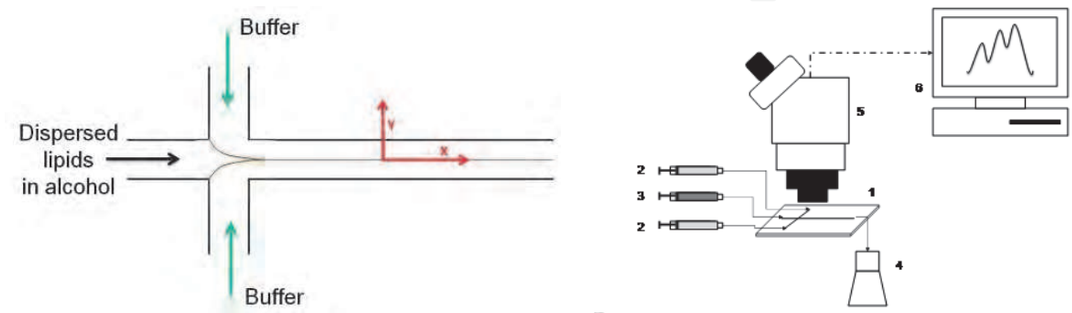

Fig. 4. (A) Schematic representation of hydrodynamic focusing (HF) in a microfluidic device with four-channel intersection geometry. The organic solvent (miscible in water) containing the dispersed lipids is injected in the middle stream and hydrodynamically compressed by two aqueous (or buffered) streams. The flow is in the x direction and alcohol diffusion is in the y direction. (B) Schematic representation of the experimental apparatus for liposome production using HF: (1) microfluidic device; (2) water syringe pumps; (3) syringe pump for lipids/ethanol stream; (4) collector flask; (5) stereo microscopy; (6) computer data acquisition (adapted from Zhang et al., 2008).

The lipid concentration in alcohol is also another important parameter for controlling size. The development of vaccines for *in vivo* applications requires the highest drug-loading capacity. In terms of gene vaccines, the DNA-loading capacity correlates with the cationic lipid content, defined by the molar charge rate ($R_{+/-}$) between the cationic charges (from the cationic lipid) and negative charges (from the DNA). The $R_{+/-}$ and total lipid content are project parameters for scaling up (or scaling out) processes. As an example, the $R_{+/-}$ of the tuberculosis gene vaccine is 10 and the total lipid concentration 64 mM (Rosada et al., 2008). These parameters require cationic liposome production in a high lipid concentration under unusual microfluidic conditions. Aiming to explore the effect of lipid concentration on microfluidic HF processes, we investigated the influence of high lipid content (100 mM) and lipid composition in ethanol (EPC or EPC/DOTAP/DOPE) as a function of average size. We understand that the studied molar concentration is greater than the lipid solubility in ethanol (approximately 4 mM for EPC) (New, 1990) and, in this case, the lipid dispersion offers an additional barrier to ethanol diffusion into water. Based on this assumption, we simulated the required microchannel length for complete ethanol diffusion from a central stream (after HF) as a function of the lipid concentration in the ethanol stream considering

the mass continuity equation (according to Figure 4A), without a chemical reaction (Equation 18). This simulation was performed based on a microfluidic glass device produced by the wet photolithographic process. The microchannels were etched with HF solution; upstream channels measured 140 ± 1 μm in width and downstream channels 200 ± 1 μm after the T junction. The microchannel was 50 ± 2 μm deep and the diffusion length 5 cm.

$$\frac{\partial C_E}{\partial t} + \left(v_x \frac{\partial C_E}{\partial x} + v_y \frac{\partial C_E}{\partial y} + v_z \frac{\partial C_E}{\partial z} \right) = D_{EW} \left(\frac{\partial^2 C_E}{\partial x^2} + \frac{\partial^2 C_E}{\partial y^2} + \frac{\partial^2 C_E}{\partial z^2} \right) \quad (18)$$

Where D_{EW} is the ethanol diffusion coefficient in water and C_E is the ethanol concentration. The Cartesian coordinates are used because the microchannel area presents rectangular geometry. Considering laminar flow in x direction and mass transfer along the y direction (Figure 4A), Equation 18 can be adapted for short times according to the Higbie penetration model (Higbie, 1935):

$$N_E = \sqrt{\frac{4.D_{EA}}{\pi.t}}.(C_{E_0} - C_{E\infty}) \quad (19)$$

Where *t* is the quotient between the difference in flow rates (water and ethanol) and distance x. The influence of lipid concentration was considered an additional barrier for ethanol diffusion due to the presence of lipid aggregates dispersed in the ethanol stream. In this case, the ethanol diffusion depends on the concentration gradient through ethanol/water streams, as well as its hydrophobic characteristics, with similar behavior as ethanol diffusion from aqueous solution to a phospholipid bilayer (Galindo-Rodriguez et al., 2004). The hydrophobic characteristics of the lipid can be expressed as the partition coefficient octanol/water ($P_{o/w}$= 0,478). In this context, D_{EW} was corrected by the partition coefficient according to Equation 20.

$$D_{EW'} = 0,478 * D_{EW} \quad (20)$$

Where $D_{EW'}$ is the effective diffusion coefficient.
Figure 5 presents the simulation of the distance (x) for total ethanol diffusion as a function of ethanol flow rate (at a fixed FRR of 6.26 and 20). Increasing the lipid concentration in the ethanol stream, the distance x to complete ethanol diffusion will increase.

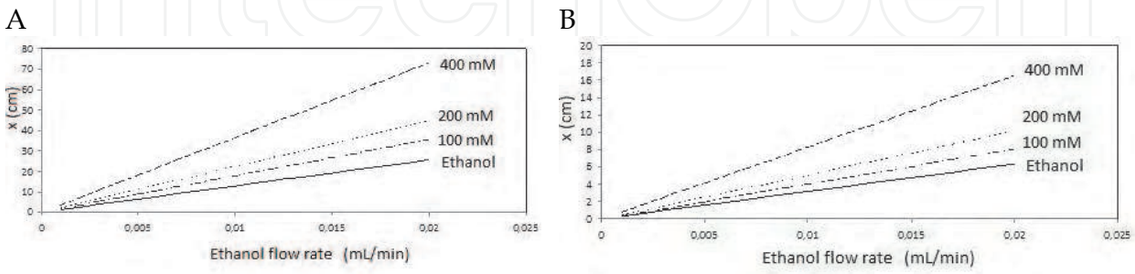

Fig. 5. Simulation of the distance for total ethanol diffusion into the water stream. The lipid (EPC) concentration was considered as an additional barrier to ethanol diffusion. (A) FRR = 6.26. (B) FRR = 20.

According to the simulation, ethanol dispersion requires the lowest length for ethanol diffusion for a lipid concentration of 100 mM (among the simulated concentrations). Experimental evaluations with this lipid concentration were performed at different total flow velocities (total flow rate) and lipid compositions (EPC and EPC/DOTAP/DOPE – cationic liposomes) as presented in Table 1. The average diameter is strongly influenced by the total flow velocity and lipid composition. Decreasing the flow velocity decreases the average size, and this behavior is not dependent on the FRR. This parameter is associated with the residence time inside the microchannel, suggesting that higher residence time is required to control liposome size. Another interesting parameter is the lipid composition. The viscosity of the ethanol dispersion was 1.07 and 1.21 cP for EPC/DOTAP/DOPE and EPC, respectively. Lower viscosity probably offers lower mass transfer resistence, reflecting smaller diameters (and standard deviations) and polydispersity index values. This difference reflected in HF is confirmed by stereomicroscopic observation along the microchannel. A high polydispersity index (Table 1) can also indicate the possibility for further process optimization in terms of flow velocity, FRR, and lipid concentration.

Lipid composition	Total flow velocity (cm/min)	FRR	Z-average (nm)	Polidispersity index
EPC	5.6	6	342.8 ± 134.5	0.427 ± 0.140
	4	7	271.6 ± 37.5	0.408 ± 0.145
EPC/DOTAP/DOPE	8.1	10.6	162.1 ± 88.13	0.606 ± 0.157
	6.1	7.7	92.92 ± 10.14	0.441 ± 0.028

FRR: volumetric flow buffer/alcohol rate-ratio.
Total lipid concentration of 100 mM in ethanol stream.

Table 1. Average liposome size (Z-average) obtained at different lipid compositions and flow rates.

4.2 Microfluidic systems for electrostatic complexation of DNA

The electrostatic interactions between DNA and cationic liposomes produce particles with different sizes and morphology (Mannisto et al., 2002; Oberle et al., 2000) that depend on $R_{+/-}$, buffer ionic strength, order of component addition, reaction conditions, and the type of lipids (Mount et al., 2003; Zelphati et al., 1998). In this context, HF can also be used to control the diffusion process for DNA compaction, producing well organized aggregates. The flow velocity is the major parameter controlling the aggregation process (Dootz et al., 2006).

Otten et al. (2005) investigated the HF microfluidic device to produce cationic liposome-DNA complexes (Figure 6). The DNA solution is introduced in the central stream and the cationic liposome stream introduced at a lateral position. The average liposome size was 200 nm (composed of 1:1 DOTAP and DOPC with a lipid concentration of 25 $mg.mL^{-1}$), and the DNA was calf thymus (5 $mg.mL^{-1}$). The flow velocity was 100 $mm.s^{-1}$, varying with $v_{Liposome} = 13v_{DNA}$ and $v_{Lipossomas} = 130v_{DNA}$, where v is the flow velocity. The authors concluded that the complex is formed in two steps. The first step relates to the formation of a multilamellar complex, followed by the second step in which DNA is organized inside the lamellae. The central stream can be focused according the FRR, and reducing the diffusional length allows faster mixing (Knight et al., 1998).

A micromixer (Jellema et al., 2010) and multi-inlet microfluidic HF (MF) system (Koh et al., 2010) were recently investigated as alternatives for producing the liposome-DNA complexes. These studies point out new and promising alternatives aiming to control the aggregation process between DNA and cationic liposomes.

5. Physico-chemical aspects

The processes that use top-down strategies for liposome production differ according to the remotion of solvent and/or application of shear. The remotion of solvent is carried out by evaporation (Bangham´s method or multitubular system), spray drying or evaporation in reverse phase, sublimation (dehydration–hydration), or solubilization in water by ether/ethanol injection in diluted or concentrated phases. The incomplete remotion of solvent has a direct impact on liposome size.

We have observed that the presence of organic solvent in spray-dried lipid structures generates more amorphous or more crystalline domains due to the packing of lipids in the bilayers (Alves and Santana, 2004). The operational conditions interfere with the drying rate, and mass transfer limitations result in the complete evaporation of ethanol. The higher the evaporation rate, the higher the amount of ethanol remaining inside the particles because a shield of packed lipids close to the surface and more amorphous structures are formed. At a slower rate of evaporation, it is more controlled, generating more crystalline structures. The subsequent hydration of the solid particles with different levels of crystallinity influences the size and polydispersity of the generated liposomes.

Similar mass transfer limitations are present when the organic solvent is removed by diffusion in water. A compromise between the diffusion and vesiculation rates controls particle size. The opposite rates of diffusion and hydration depend on the barrier created by the phospholipids, which is a function of its concentration and depends on the interaction among lipids. In previous studies, we characterized the packing of pseudo-ternary mixed Langmuir monolayers of EPC/DOTAP/DOPE using surface–molecular area curves. The interactions and miscibility behavior were inferred from the curves by calculating the excess free energy of the mixture (ΔG_{Exc}). The deviation from ideal showed dependence on the lipid polar head type and monolayer composition (Rigoletto et al., 2011).

The rates of vesiculation and solvent diffusion are comparable in magnitude only at very low lipid concentrations, generating small liposomes in an excess of water. Under other conditions, the barrier created by the extension of the primary aggregation of lipids delays solvent remotion, generating large multilamellar liposomes. Otherwise, the rate of vesiculation is associated with the hydrophobicity of the non-polar groups. Therefore, the vesiculation rate in the primary aggregate controls liposome size. When cationic lipids are used, such as in the DOTAP/DOPE/EPC system, the electrostatic repulsion among the molecules benefits solvent diffusion and hydration, generating smaller liposomes.

Because of the softness of the primary aggregate and the bilayer fluidity imparted by the phase transition temperature, liposomes are prone to fusion due to the non-ordered Brownian movement of the colloids in the medium, and multilamellar vesicles are generated in a broad range of sizes. The remaining solvent generates polydispersed liposomes, which are more favorable for fusion. However, charged lipids stabilize liposomes. Therefore, mass transfer is critical in discontinuous processing, controlling liposome size and polydispersity.

Despite limitations in mass transfer and interactions, discontinuous processes are still preferable due to the simplicity in carrying out massive liposome production and scaling up

processes. In this context, the development of technologies that promote the production of cationic liposomes with controlled size and low polydispersity index, with low energy consumption and the elimination of organic solvents, is still a challenge.
Continuous processes in microchannels with HF reduce the limitations due to mass transfer in the interface of the primary aggregate, and the continuous operation decreases interactions among particles due to Brownian movement. Therefore, particle size is controlled by the relative flow rates between the phases and by microchannel length.

6. A case study of the production of cationic liposomes and gene vaccines in scalable top-down processing

Although top-down strategies are important and high shear processing has various uses, no systematic studies have been carried out on the effects of liposome comminution on the physico-chemical and surface properties of liposomes. The data in the literature are sparse in regards to the kind of impellers, comminution equipment, or type of lipids used.
Aiming to produce the gene vaccine composed of EPC/DOTAP/DOPE liposomes with DNA complexed on their external surface, we initially studied the significance of the process variables for the properties of liposomes composed of egg lecithin. Mechanical forces were used for homogenation and comminution in Caules type stirrer, Ultra-Turrax, and microchannel microfluidizer equipment. A main variable was selected and its effects on the physico-chemical properties of the liposomes characterized. Finally, a scalable discontinuous process was established and EPC/DOTAP/DOPE liposomes produced and complexed with DNA. The physico-chemical and biological properties of the gene vaccine were compared with our previous gene vaccine prepared using Bangham's method.

6.1 Effects of the process variables on liposome properties

6.1.1 Statistical analysis

We studied the effects of the shear rate using multi-factorial statistical experimental planning (Montgomery 2008) in order to delineate the relative importance and influence of the shear rate and feed flow rate on the mean diameter, polydispersity, zeta potential, and viscosity of egg lecithin liposomes. The liposomes were prepared with high lipid concentration (300 mM), aiming for applications in scaling up processes. Food grade egg lecithin (60% phosphatidylcholine content) from Degussa (GmbH Germany) and ethanol 99-100% from Labsynth ltda. (São Paulo- Brazil) were used as the lipid and solvent, respectively.
Figure 7 shows the experimental outline for liposome preparation. The 300 mM ethanol-lipid suspension in a beacker (1) was fed at a previously defined flow rate through a peristaltic pump (2) into the bottom of a 150 mL beaker with four fins containing pure Milli Q water (3). Continuous mechanical stirring was provided by a Caules type stirrer or Ultra-Turrax® IKA T25 (Ika Works) (4). The final lipid concentration was 50 mM. After the feeding was complete, stirring was maintained for an additional 15 min. Comminution was also carried out in a microchannel microfluidizer (Microfluidizer® M-110P) with 100 mL of a liposome dispersion pre-processed through an Ultra-Turrax® at 5000 to 21000 s^{-1} shear rate and 0.09 to 0.96 $mL.s^{-1}$. The microfluidizer worked in the pressure range of 200 to 1500 bar and for various passages. All liposome dispersions were stored at 8°C for 12 hours before characterization.

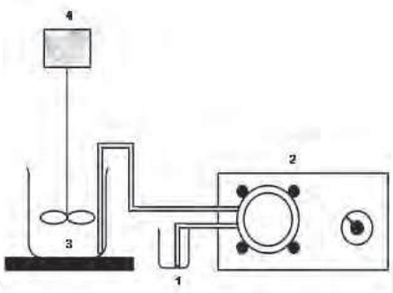

Fig. 7. Scheme of the experimental set-up used for liposome preparation using (A) Ultra-Turrax® or Caules mechanical stirrer. 1) Tank containing the lipid dispersion in ethanol; 2) peristaltic pump; 3) tank with four fins containing (150 mL) water; 4) Ultra-Turrax® or Caules mechanical stirrer. (B) Microchannel microfluidizer system processed the samples from the Ultra-Turrax®.

6.1.2 Significance of shear and feed flow rates

The effects of the shear rate and feed flow rate on the mean diameter, polydispersity, and zeta potential are presented in Table 2 and in terms of the significance of the independent variables and their interaction in the Pareto graphics in Figure 8. For the Caules type stirrer, the effects of shear rate and feed flow rate on the mean diameter of liposomes were not significant (Figure 8A1). The shear rate was significant for polydispersity (Figure 8A2), and both variables were significant for zeta potential (Figure 8A3). The interactions between the variables were not significant for the three response variables.

Table A

Factors	-	0	+
1: Shear rate (s^{-1})	2,860	12,140	21,430
2: Inlet lipid solution flow rate (mL/s)	0.09	0.54	0.96

Experiment	1	2	Diameter (nm)	Polydispersity	Zeta Potential (mV)
1	-1	-1	386.10	0.37	-53.73
2	1	-1	254.73	0.31	-56.33
3	-1	1	550.20	0.58	-53.73
4	1	1	246.50	0.35	-48.57
5	0	0	374.83	0.47	-55.90
6	0	0	359.00	0.36	-54.60
7	0	0	358.90	0.45	-54.40

Table B

Factors	-	0	+
1: Shear rate (s^{-1})	1,000	1,750	2,530
2: Inlet lipid solution flow rate (mL/s)	0.09	0.54	0.96

Experiment	1	2	Diameter (nm)	Polydispersity	Zeta Potential (mV)
1	-1	-1	626.17	0.65	-55.00
2	1	-1	414.87	0.51	-71.27
3	-1	1	616.47	0.68	-57.50
4	1	1	446.77	0.51	-52.60
5	0	0	582.77	0.65	-57.27
6	0	0	642.67	0.58	-55.80
7	0	0	567.40	0.62	-56.00

Table 2. (A,B) Physico-chemical properties of liposomes as a function of the operational variables.

Data obtained using ultra-turrax showed a significant influence of the shear and feed flow rates, as well as their interactions, on the mean diameter and polydispersity (Figure 8B1,B2). However, these variables had no significant effect on the zeta potential (Figure 8B3). The mean diameter was influenced more by shear rate, whereas both shear rate and feed flow rate were significant for polydispersity.

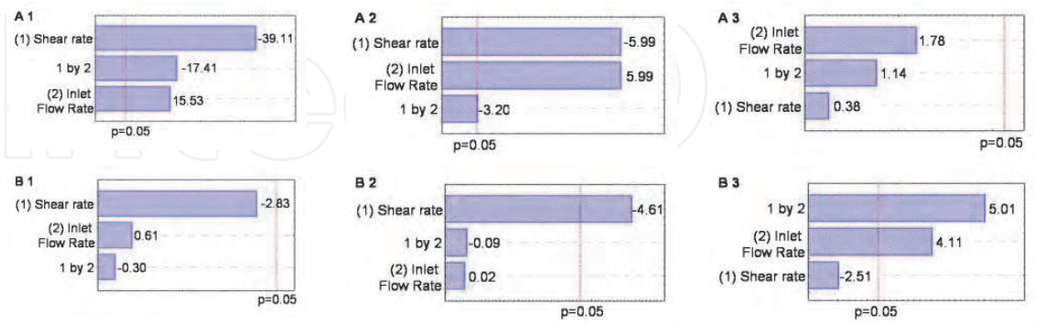

Fig. 8. Pareto´s graphic for liposome production using (A) Caules and (B) Ultra-Turrax® stirrers. (A1,B1) mean diameter hidrodinâmico médio cumulativo, (A2,B2) polydispersity, (A3,B3) zeta potential.

The results show that the shear rate range of the Caules stirrer did not comminute the aggregates less than 600 nm in size, but it destroyed the progressive aggregations, influencing the polydispersity and zeta potential. However, the higher shear rates provided by the ultra-turrax better control phospholipid aggregation, generating smaller liposomes. Control is strongly dependent on the intensity of shear, and sizes in the range of 200 nm were obtained at the superior shear rate limit (21530 s^{-1}) provided by the equipment. Feed flow rate influence mainly occurs at the inferior shear rate limit (2860 s^{-1}). Though the shear rate range for ultra-turrax interferes with primary liposome aggregation, the zeta potential is not influenced. Therefore, for egg lecithin (300 mM concentration) liposomes, the shear rate range between 1000 and 21430 s^{-1} delimits the liposome size from approximately 600 to 200 nm.

6.1.3 Effects of the shear rate on the liposome properties

Mean diameter - Additional data allowed the construction of the curve presented in Figure 9A. The curve shows a clear relationship between liposome comminution and shear rate, with the mean diameter exponentially decaying with applied shear rate. The error bars are higher at lower shear rates due to the poor homogenization of liposomes provided by the lower pumping capabilities of the mechanical systems.

The microchannel microfluidizer, working in the pressure range of 200 to 1500 bars, provided shear rates in the range of 2×10^5 to 6×10^5 s^{-1} .The data from the microchannel microfluidizer were obtained for pre-treated liposomes using Ultra-Turrax at shear and feed flow rates of 5600 to 24000 s^{-1} and 0.09 to 0.96 $mL.s^{-1}$, respectively. The results show that the pre-formed liposomes reached the nanometric range (100 nm) in only one passage using Ultra-Turrax and the high shear rate range of the microchannel microfluidizer.

This comminution behavior agrees with the results reported by Diat et al. (1993a). Through a balance between elastic and viscous forces in the liposomes, the mean diameter is reduced according to the square root of the applied shear rate (Equation 21).

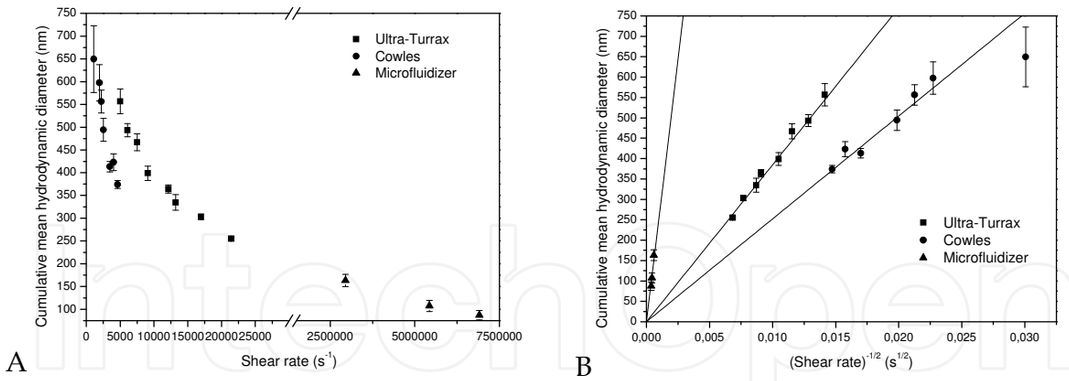

Fig. 9. Cumulative hydrodynamic mean diameter as a function of the shear rate provided by Caules stirrer, Ultra-Turrax®, or microchannel microfluidizer. (A) Z-average values obtained from light scattering measurements. (B) Linear relationship from Equation 21 proposed by Diat et al. (1993a).

$$R = \sqrt{\frac{4.\pi.\left(2.k + \bar{k}\right)}{\mu.d.\dot{\gamma}}} \tag{21}$$

Where R is the liposome radius at equilibrium, k and k are the average and Gaussian elastic constant of the membrane, respectively, μ is the viscosity of the liposome dispersion, $\dot{\gamma}$ is the shear rate, and d is the interlamellar distance. The different slopes for the straight lines in Figure 9B were obtained for the shear rate ranges of the devices used, agreeing with the mass balance between elastic and viscous forces in the liposomes described by Diat et al. (1993b). Higher shear rates produce higher slopes, indicating the presence of liposomes with higher elastic constant, lower viscosity, and shorter interlamellar distance.

6.1.3.1 Viscosity, surface tension, and zeta potential

The shear rate also reduced the viscosity of the liposome dispersion from 5 to 2 mPa, but no significant changes were observed in the surface tension as a consequence of the reduction in size. However, the reduction in size also resulted in rearrangement of the lipids in the external layer, changing the zeta potential from -50 to -40 mV.

6.1.3.2 Lamellar packing

Small angle X-ray scattering (SAXS) characterization showed changes in the interlamellar distances for the applied shear rate ranges (Figure 10). The distance decreased with higher shear rates. The decreasing interlamellar distance was a consequence of the loss of interlamellar water, calculated to be up to 12% for the highest level of shear rate, as well as of lipid packing in the liposome, found to be less than 2%. The water layer is calculated as the difference between the full period and the bilayer thickness (see Table 4). These factors may explain the observed changes in zeta potential and the different slopes of the straight lines obtained for the studied shear rate ranges. In addition to the interlamellar distance and packing, the elasticity of the bilayer may also be influenced by the shear rate and changes in the elastic constants determined. In general, elastic modulus is not the same as stiffness. Elastic modulus is a property of the constituent material, whereas stiffness is a property of the structure. In the case of liposomes, the elastic modulus is an intensive property of the

lipids, and stiffness is an extensive property dependent on the structure and packing of the aggregate. Therefore, we associated the changes in the slope of the straight lines in Figure 9B with changes in the elastic constants as a consequence of the changes in packing in the liposomes.

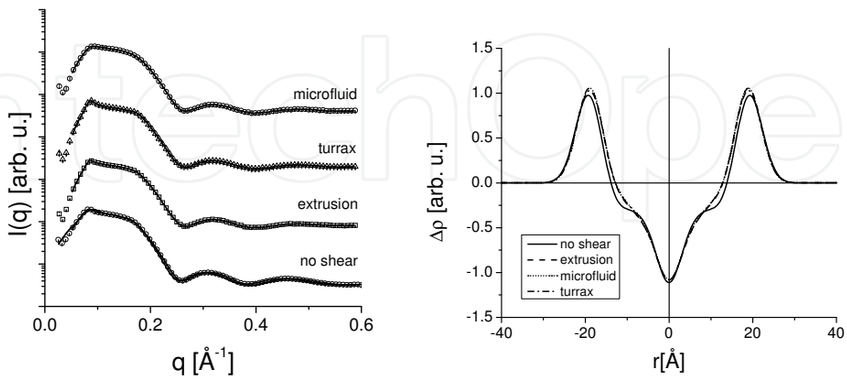

Fig. 10. Left: Small angle X-ray scattering (SAXS) profiles determined for the liposomes treated under moderate shear (extruded through polycarbonate membranes) and high shear produced by Ultra-Turrax® (21430 s^{-1}) and microchannel microfluidizer devices (6 961 000 s^{-1}). Right: Electron density profile across the bilayer obtained from the fitting (see Table 3).

Sample	Period[Å]	Bilayer thickness[Å]	N	η
no shear	76.7±0.2	59,9±0.1	3.2±0.1	0.18±0.02
Extrusion	73.4±0.1	59,3±0.1	3.4±0.1	0.26±0.01
Turrax	72.5±0.2	59,1±0.1	4.1±0.1	0.26±0.01
Microfluid	72.3±0.1	59,2±0.2	2.3±0.1	0.09±0.01

***N** is the average number of bilayers and **η** is the Caillé parameter.*

Table 3. Structural parameters obtained from full curve modeling of SAXS data.

6.1.3.3 Morphology

Figure 11 presents transmission electronic microscope images of the liposomes under various shear treatments compared to control (Bangham's method).

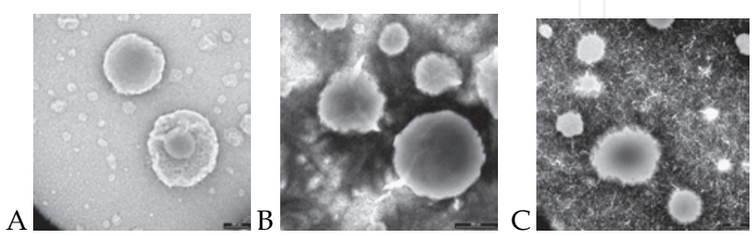

Fig. 11. Transmission electronic microscopy of liposomes obtained using (A) Bangham's method followed by extrusion in membranes, (B) ultra-turrax under a shear rate of 21430 s^{-1}, (C) microchannel microfluidizer under a shear rate 6 961 000 s^{-1}. Bars :200nm

Under low shear, the liposome surface looks thicker (Figure 11A), whereas it looks more packed with ultra-turrax treatment (Figure 11B). However, in both cases the liposome morphology is spherical. Under the highest shear, the morphology of the liposomes was not spherical, and irregularities in the surface reflect stretching of the aggregated structure (Figure 8C). These results reflect the observed change in packing and zeta potential as a consequence of the shear rate.

6.1.4 Scalable top-down process for liposome production

The scalable process described in Figure 12 was established based on these results and validated for the production of EPC/DOPE/DOTAP liposomes. Previous assays (data not shown) validated the changes in the purity of EPC from 99-100% (analytical grade) to 96-98% (commercial grade) and the lipid concentration from 16 mM (used in the Bangham's method) to 64 mM.

The injection of ethanol was used modified for the higher lipid concentration. Lipid concentration in the ethanol phase was previously optimized with an aim to minimize the concentration of ethanol in the liposome formulation, as well as prevent obstructions of the microchannels in the microfluidizer.

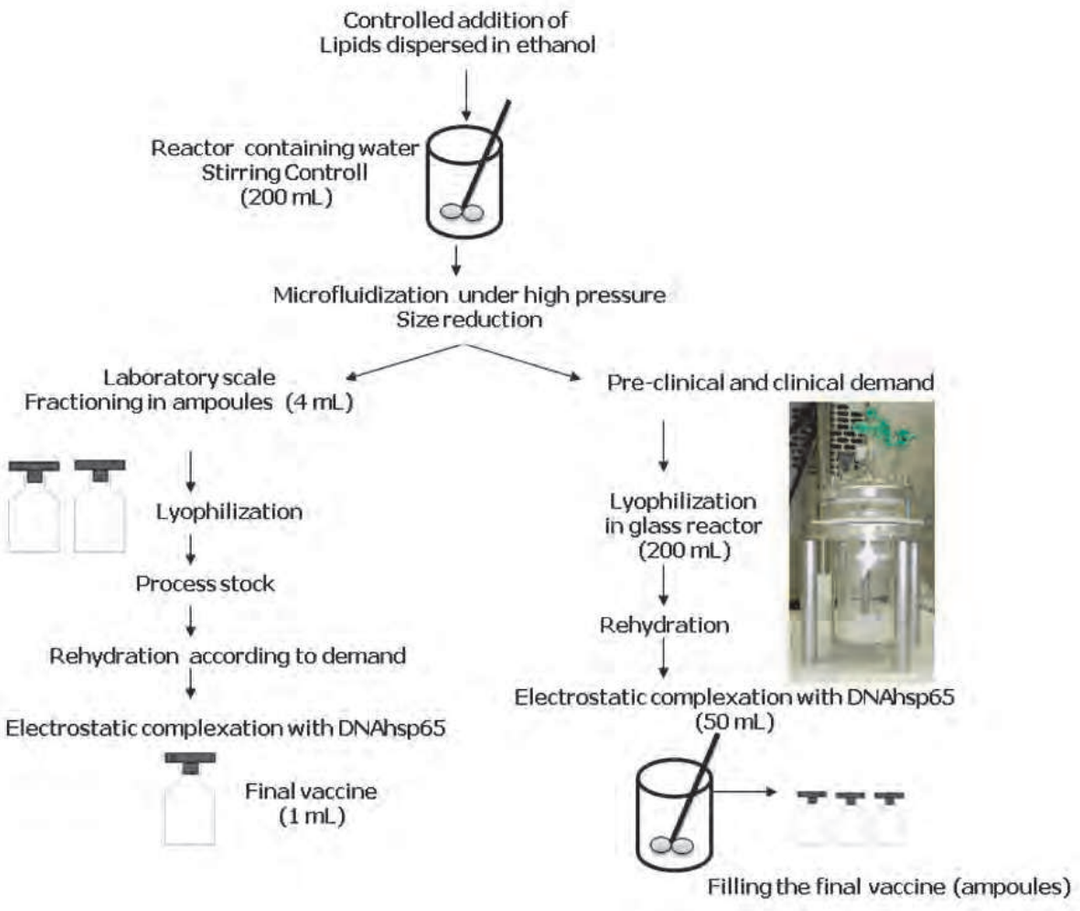

Fig. 12. Schematic diagram of the scalable process for cationic liposome production.

7. Conclusions

The top-down and bottom-up approaches are valuable for liposome production. By understanding the physico-chemical aspects and behavior of variables involved in the process, we can establish a conscious scalable process for liposome production and connect functional liposomes, the performance of the production process, and the final properties of the gene vaccine as a product. The results presented in this chapter open opportunities for the development of new gene or non-gene vaccines in future research using scalable top-down and bottom-up processes.

8. Acknowledgment

The authors acknowledge the University of Campinas, the Brazilian Synchrotron Light National Laboratory, and the financial agencies FAPESP and CNPq in Brazil.

9. References

Alves, G. P., and Santana, M. H. A. (2004) Phospholipid dry powders produced by spray drying processing: Structural, thermodynamic and physical properties, *Powder Technology*, Vol. 145, pp 139-148, ISSN 0032-5910.

Azaroff, L. V. (1968) *Elements of x-ray crystallography*, McGraw Hill Book, New York.

Baldas, L., and Caen, R. (2010) Experimental methods *in: Microfluidics*, Vol. Edited by Stéphane Colin, pp 330-348.

Bangham, A. D., Standish, M. M., and Watkins, J. C. (1965) Diffusion of univalent ions across lamellae of swollen phospholipids, *Journal of Molecular Biology*, Vol. 13, p 238, ISSN 0022-2836.

Caille, A. (1972) *C. R. Seances Acad. Sci. B*, Vol. 274, p 891, ISSN 0249-6313.

Ciccariello, S., and Sobry, R. (1999) Small-angle scattering intensity behaviours of cylindrical, spherical and planar lamellae, *Journal of Applied Crystallography*, Vol. 32, pp 892-901, ISSN 0021-8898.

Cullity, B. D. (1978) *Elements of x ray diffraction*, 2nd ed., Addison Wesley, USA.

de Paula, L., Silva, C. L., Carlos, D., Matias-Peres, C., Sorgi, C. A., Soares, E. G., Souza, P. R., Blades, C. R., Galleti, F. C., Bonato, V. L., Goncalves, E. D., Silva, E. V., and Faccioli, L. H. (2007) Comparison of different delivery systems of DNA vaccination for the induction of protection against tuberculosis in mice and guinea pigs, *Genet Vaccines Ther*, Vol. 5, p 2, ISSN 1479-0556.

Diat, O., and Roux, D. (1993a) Preparation of monodisperse multilayer vesicles of controlled size and high encapsulation ratio, *Journal De Physique II*, Vol. 3, pp 9-14, ISSN 1155-4312.

Diat, O.; Roux, D.; Nallet, F. (1993b) Effect of Shear on a Lyotropic Lamellar Phase. *Journal de Physique II*, Vol.3, pp. 1427-1452.

Dootz, R., Otten, A., Koster, S., Struth, B., and Pfohl, T. (2006) Evolution of DNA compaction in microchannels, *Journal of Physics-Condensed Matter*, Vol. 18, pp S639-S652, ISSN 0953-8984.

Egelhaaf, S. U., Wehrli, E., Muller, M., Adrian, M., and Schurtenberger, P. (1996) Determination of the size distribution of lecithin liposomes: A comparative study using freeze fracture, cryoelectron microscopy and dynamic light scattering, *Journal of Microscopy-Oxford*, Vol. 184, pp 214-228, ISSN 0022-2720.

Fritz, G., and Glatter, O. (2006) Structure and interaction in dense colloidal systems: Evaluation of scattering data by the generalized indirect fourier transformation method, *Journal of Physics: Condensed Matter*, Vol. 18, pp S2403-S2419, ISSN 0953-8984.

Galindo-Rodriguez, S., Allemann, E., Fessi, H., and Doelker, E. (2004) Physicochemical parameters associated with nanoparticle formation in the salting-out, emulsification-diffusion, and nanoprecipitation methods, *Pharmaceutical Research*, Vol. 21, pp 1428-1439, ISSN 0724-8741.

Glatter, O. (1982) Data treatment, In *Small angle x ray scattering* (Glatter, O. & Kratky, O., Eds.), p 137, Academic Press, London.

Glatter, O. (1991) Scattering studies on colloids of biological interest (amphiphilic systems), In *Trends in colloid and interface science v* (Corti, M. & Mallamace, F., Eds.), pp 46-54, Springer Berlin / Heidelberg.

Glatter, O. (2002) Neutrons, x-rays and light: Scattering methods applied to soft condensed matter, In *Static light scattering of large systems* (Lindner, P. & Zemb, T., Eds.), pp 171-201, Elsevier, ISBN 0-444-51122-9, Amsterdam.

Glatter, O., and Kratky, O., (Eds.) (1982) *Small angle x ray scattering*, Academic Press, London.

Gregoriadis, G. (1993) *Liposome technology*, CRC Press, Inc, ISBN 0-8493-6709-3.

Higbie, R. (1935) The rate of absorption of a pure gas into a still liquid during short periods of exposure, *Transactions of the American Institute of Chemical Engineers*, Vol. 31, pp 365-389, ISSN 0096-7408.

Hsieh, A. T. H., Hori, N., Massoudi, R., Pan, P. J. H., Sasaki, H., Lin, Y. A., and Lee, A. P. (2009) Nonviral gene vector formation in monodispersed picolitre incubator for consistent gene delivery, *Lab on a Chip*, Vol. 9, pp 2638-2643, ISSN 1473-0197.

Hulst, H. C. v. d. (1957) *Light scattering by small particles*, Wiley, New York.

Jahn, A., Reiner, J. E., Vreeland, W. N., DeVoe, D. L., Locascio, L. E., and Gaitan, M. (2008) Preparation of nanoparticles by continuous-flow microfluidics, *Journal of Nanoparticle Research*, Vol. 10, pp 925-934, ISSN 1388-0764.

Jahn, A., Stavis, S. M., Hong, J. S., Vreeland, W. N., Devoe, D. L., and Gaitan, M. (2010) Microfluidic mixing and the formation of nanoscale lipid vesicles, *Acs Nano*, Vol. 4, pp 2077-2087, ISSN 1936-0851.

Jahn, A., Vreeland, W. N., DeVoe, D. L., Locascio, L. E., and Gaitan, M. (2007) Microfluidic directed formation of liposomes of controlled size, *Langmuir*, Vol. 23, pp 6289-6293, ISSN 0743-7463.

Jahn, A., Vreeland, W. N., Gaitan, M., and Locascio, L. E. (2004) Controlled vesicle self-assembly in microfluidic channels with hydrodynamic focusing, *Journal of the American Chemical Society*, Vol. 126, pp 2674-2675, ISSN 0002-7863.

Jellema, R. K., Bomans, P., Deckers, N., Ungethum, L., Reutelingsperger, C. P. M., Hofstra, L., and Frederik, P. M. (2010) Transfection efficiency of lipoplexes for site-directed delivery, *Journal of Liposome Research*, Vol. 20, pp 258-267, ISSN 0898-2104.

Knight, J. B., Vishwanath, A., Brody, J. P., and Austin, R. H. (1998) Hydrodynamic focusing on a silicon chip: Mixing nanoliters in microseconds, *Physical Review Letters*, Vol. 80, pp 3863-3866, ISSN 0031-9007.

Koh, C. G., Zhang, X. L., Liu, S. J., Golan, S., Yu, B., Yang, X. J., Guan, J. J., Jin, Y., Talmon, Y., Muthusamy, N., Chan, K. K., Byrd, J. C., Lee, R. J., Marcucci, G., and Lee, L. J. (2010) Delivery of antisense oligodeoxyribonucleotide lipopolyplex nanoparticles assembled by microfluidic hydrodynamic focusing, *J. Control. Release*, Vol. 141, pp 62-69, ISSN 0168-3659.

Kratky, O. (1988) The importance of x-ray small-angle scattering in colloid research, In *Dispersed systems* (Hummel, K. & Schurz, J., Eds.), pp 1-14, Springer Berlin / Heidelberg.

Kratky, O., and Laggner, P. (2001) X-ray small-angle scattering, In *Encyclopedia of physical science and technology* (Robert, A. M., Ed.), pp 939-988, Academic Press, ISBN 978-0-12-227410-7, New York.

Kremer, J. M. H., Esker, M. W. J., Pathmamanoharan, C., and Wiersema, P. H. (1977) Vesicles of variable diameter prepared by a modified injection method, *Biochemistry*, Vol. 16, pp 3932-3935, ISSN 0006-2960.

Lasic, D. D. (1993) *Liposomes: From physics to applications*, Amsterdam:Elsevier Science Publishers B.V.

Mannisto, M., Vanderkerken, S., Toncheva, V., Elomaa, M., Ruponen, M., Schacht, E., and Urtti, A. (2002) Structure-activity relationships of poly(l-lysines): Effects of pegylation and molecular shape on physicochemical and biological properties in gene delivery, *J. Control. Release*, Vol. 83, pp 169-182, ISSN 0168-3659.

Mijatovic, D., Eijkel, J. C. T., and van den Berg, A. (2005) Technologies for nanofluidic systems: Top-down vs. Bottom-up - a review, *Lab on a Chip*, Vol. 5, pp 492-500, ISSN 1473-0189.

Montgomery, D. C. (2008) *Design and analysis of experiments*, John Wiley & Sons.

Mount, C. N., Lee, L. K., Yasin, A., Scott, A., Fearn, T., and Shamlou, P. A. (2003) The influence of physico-chemical and process conditions on the physical stability of plasmid DNA complexes using response surface methodology, *Biotechnology and Applied Biochemistry*, Vol. 37, pp 225-234, ISSN 0885-4513.

Nagle, J. F., Zhang, R., Tristram-Nagle, S., Sun, W., Petrache, H. I., and Suter, R. M. (1996) X-ray structure determination of fully hydrated l alpha phase dipalmitoylphosphatidylcholine bilayers, *Biophys J*, Vol. 70, pp 1419-1431, ISSN 0006-3495.

Nallet, F., Laversanne, R., and Roux, D. (1993) Modelling x-ray or neutron scattering spectra of lyotropic lamellar phases : Interplay between form and structure factors, *J. Phys. II France*, Vol. 3, pp 487-502.

New, R. R. C. (1990) *Liposomes: A practical approach (the practical approach series)*.

Oberle, V., Bakowsky, U., Zuhorn, I. S., and Hoekstra, D. (2000) Lipoplex formation under equilibrium conditions reveals a three-step mechanism, *Biophysical Journal*, Vol. 79, pp 1447-1454, ISSN 0006-3495.

Ogris, M., Steinlein, P., Kursa, M., Mechtler, K., Kircheis, R., and Wagner, E. (1998) The size of DNA/transferrin-pei complexes is an important factor for gene expression in cultured cells, *Gene Therapy*, Vol. 5, pp 1425-1433, ISSN 0969-7128.

Oliveira, C. L. P., Sankar R., Kloesgen, M. B., and Pedersen, J. S. (Unpublished work).

Ota, S., Yoshizawa, S., and Takeuchi, S. (2009) Microfluidic formation of monodisperse, cell-sized, and unilamellar vesicles, *Angewandte Chemie-International Edition*, Vol. 48, pp 6533-6537, ISSN 1433-7851.

Otten, A., Koster, S., Struth, B., Snigirev, A., and Pfohl, T. (2005) Microfluidics of soft matter investigated by small-angle x-ray scattering, *Journal of Synchrotron Radiation*, Vol. 12, pp 745-750, ISSN 0909-0495.

Pabst, G., Rappolt, M., Amenitsch, H., and Laggner, P. (2000) Structural information from multilamellar liposomes at full hydration: Full q-range fitting with high quality x-ray data, *Physical Review E*, Vol. 62, p 4000.

Pachence, J. M., and Blasie, J. K. (1991) Structural investigation of the covalent and electrostatic binding of yeast cytochrome c to the surface of various ultrathin lipid multilayers using x-ray diffraction, *Biophysical journal*, Vol. 59, pp 894-900, ISSN 0006-3495.

Pedersen, J. S., Posselt, D., and Mortensen, K. (1990) Analytical treatment of the resolution function for small-angle scattering, *Journal of Applied Crystallography*, Vol. 23, pp 321-333, ISSN 0021-8898.

Perrie, Y., Frederik, P. M., and Gregoriadis, G. (2001) Liposome-mediated DNA vaccination: The effect of vesicle composition, *Vaccine*, Vol. 19, pp 3301-3310, ISSN 0264-410X.

Perrie, Y., and Gregoriadis, G. (2000) Liposome-entrapped plasmid DNA: Characterisation studies, *Biochimica Et Biophysica Acta-General Subjects*, Vol. 1475, pp 125-132, ISSN 0304-4165.

Rejman, J., Oberle, V., Zuhorn, I. S., and Hoekstra, D. (2004) Size-dependent internalization of particles via the pathways of clathrin-and caveolae-mediated endocytosis, *Biochemical Journal*, Vol. 377, pp 159-169, ISSN 0264-6021.

Rigoletto, T. D., Zaniquelli, M. E. D., Santana, M. H. A., and de la Torre, L. G. (2011) Surface miscibility of epc/dotap/dope in binary and ternary mixed monolayers, *Colloids and Surfaces B-Biointerfaces*, Vol. 83, pp 260-269, ISSN 0927-7765.

Rosada, R. S., de la Torre, L. G., Frantz, F. G., Trombone, A. P. F., Zarate-Blades, C. R., Fonseca, D. M., Souza, P. R. M., Brandao, I. T., Masson, A. P., Soares, E. G., Ramos, S. G., Faccioli, L. H., Silva, C. L., Santana, M. H. A., and Coelho-Castelo, A. A. M. (2008) Protection against tuberculosis by a single intranasal administration of DNA-hsp65 vaccine complexed with cationic liposomes, *BMC Immunol.*, Vol. 9, p 13, ISSN 1471-2172.

Ross, P. C., and Hui, S. W. (1999) Lipoplex size is a major determinant of in vitro lipofection efficiency, *Gene Therapy*, Vol. 6, pp 651-659, ISSN 0969-7128.

Sato, T., Sakai, H., Sou, K., Medebach, M., Glatter, O., and Tsuchida, E. (2009) Static structures and dynamics of hemoglobin vesicle (hbv) developed as a transfusion alternative, *J Phys Chem B*, Vol. 113, pp 8418-8428, ISSN 1520-6106.

Shimomura, M., and Sawadaishi, T. (2001) Bottom-up strategy of materials fabrication: A new trend in nanotechnology of soft materials, *Current Opinion in Colloid & Interface Science*, Vol. 6, pp 11-16, ISSN 1359-0294.

Shum, H. C., Lee, D., Yoon, I., Kodger, T., and Weitz, D. A. (2008) Double emulsion templated monodisperse phospholipid vesicles, *Langmuir*, Vol. 24, pp 7651-7653, ISSN 0743-7463.

Silva, C. L., Bonato, V. L. D., Coelho-Castelo, A. A. M., De Souza, A. O., Santos, S. A., Lima, K. M., Faccioli, L. H., and Rodrigues, J. M. (2005) Immunotherapy with plasmid DNA encoding mycobacterial hsp65 in association with chemotherapy is a more rapid and efficient form of treatment for tuberculosis in mice, *Gene Therapy*, Vol. 12, pp 281-287, ISSN 0969-7128.

Torre, L. G., Carneiro, A. L., Rosada, R. S., Silva, C. L., and Santana, M. H. A. (2007) A mathematical model describing the kinetic of cationic liposome production from dried lipid films adsorbed in a multitubular system, *Brazilian Journal of Chemical Engineering*, Vol. 24, pp 477-486, ISSN 0104-6632.

Tournier, V. H., Trionex, M. S., and Chable-Beaumont, C. G. L. (1999) Liposomes with enhanced entrapment capacity and their use in imaging, In *US Patent* (Bracco Reserach S.A, Ed.).

Wagner, A., Vorauer-Uhl, K., Kreismayr, G., and Katinger, H. (2002) The crossflow injection technique: An improvement of the ethanol injection method, *Journal of Liposome Research*, Vol. 12, pp 259-270, ISSN 0898-2104.

Wiewrodt, R., Thomas, A. P., Cipelletti, L., Christofidou-Solomidou, M., Weitz, D. A., Feinstein, S. I., Schaffer, D., Albelda, S. M., Koval, M., and Muzykantov, V. R. (2002) Size-dependent intracellular immunotargeting of therapeutic cargoes into endothelial cells, *Blood*, Vol. 99, pp 912-922, ISSN 0006-4971.

Xu, Y., Szoka, F.C.J. (1996) Mechanism of DNA release from cationic liposome/DNA complexes used in cell transfection, *Biochemistry*, Vol. 35, pp. 5616-5623, ISSN: 0006-2960.

Zelphati, O., Nguyen, C., Ferrari, M., Felgner, J., Tsai, Y., and Felgner, P. L. (1998) Stable and monodisperse lipoplex formulations for gene delivery, *Gene Therapy*, Vol. 5, pp 1272-1282, ISSN 0969-7128.

Zhang, R., Suter, R. M., and Nagle, J. F. (1994) Theory of the structure factor of lipid bilayers, *Phys Rev E Stat Phys Plasmas Fluids Relat Interdiscip Topics*, Vol. 50, pp 5047-5060, ISSN 1063-651X.

Zhang, R., Tristram-Nagle, S., Sun, W., Headrick, R. L., Irving, T. C., Suter, R. M., and Nagle, J. F. (1996) Small-angle x-ray scattering from lipid bilayers is well described by modified caille theory but not by paracrystalline theory, *Biophys J*, Vol. 70, pp 349-357, ISSN 0006-3495.

Zhang, S. B., Zhao, B., Jiang, H. M., Wang, B., and Ma, B. C. (2007) Cationic lipids and polymers mediated vectors for delivery of sirna, *J. Control. Release*, Vol. 123, pp 1-10, ISSN 0168-3659.

Zhang, S. H., Shen, S. C., Chen, Z., Yun, J. X., Yao, K. J., Chen, B. B., and Chen, J. Z. (2008) Preparation of solid lipid nanoparticles in co-flowing microchannels, *Chemical Engineering Journal*, Vol. 144, pp 324-328, ISSN 1385-8947.

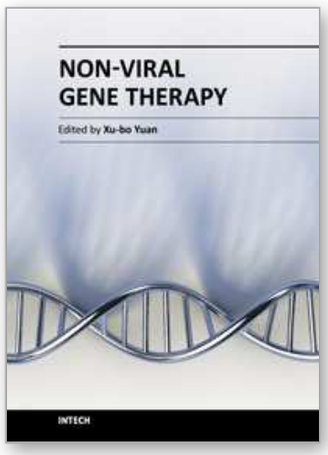

Non-Viral Gene Therapy

Edited by Prof. Xubo Yuan

ISBN 978-953-307-538-9
Hard cover, 696 pages
Publisher InTech
Published online 07, November, 2011
Published in print edition November, 2011

This book focuses on recent advancement of gene delivery systems research. With the multidisciplinary contribution in gene delivery, the book covers several aspects in the gene therapy development: various gene delivery systems, methods to enhance delivery, materials with modification and multifunction for the tumor or tissue targeting. This book will help molecular biologists gain a basic knowledge of gene delivery vehicles, while drug delivery scientist will better understand DNA, molecular biology, and DNA manipulation.

InTech Europe
University Campus STeP Ri
Slavka Krautzeka 83/A
51000 Rijeka, Croatia
Phone: +385 (51) 770 447
Fax: +385 (51) 686 166
www.intechopen.com

InTech China
Unit 405, Office Block, Hotel Equatorial Shanghai
No.65, Yan An Road (West), Shanghai, 200040, China
中国上海市延安西路65号上海国际贵都大饭店办公楼405单元
Phone: +86-21-62489820
Fax: +86-21-62489821

IntechOpen